Journal of Loss Prevention in the Process Industries 75 (2022) 104706

Contents lists available at ScienceDirect

Journal of Loss Prevention in the Process Industries

journal homepage: www.elsevier.com/locate/jlp

Analysis of pressure drop and blast pressure leakage of passive air blast safety valves: An experimental and numerical study

Lorenz Brenner [a,c], Christian Jenni [a], Flurin Guyer [a], Patrick Stähli [a], Robert Eberlein [b], Matthias Huber [b], André Zahnd [c], Martin Schneider [a], Frank Tillenkamp [a,*]

[a] Zurich University of Applied Sciences (ZHAW), Institute of Energy Systems and Fluid Engineering (IEFE), Technikumstrasse 9, CH-8401, Winterthur, Switzerland
[b] Zurich University of Applied Sciences (ZHAW), Institute of Mechanical Systems (IMES), Technikumstrasse 9, CH-8401, Winterthur, Switzerland
[c] Federal Office for Civil Protection FOCP, SPIEZ LABORATORY, Austrasse, CH-3700, Spiez, Switzerland

ARTICLE INFO

Keywords:
Passive air blast safety valve
Blast pressure leakage
Pressure drop
Optimization procedure
Numerical investigation
Experimental investigation

ABSTRACT

The purpose of passive air blast safety valves is to protect people and technical installations in buildings or facilities. In case of explosions, e.g. due to technical failures in an oil- and gas refinery, the safety valve should close in milliseconds with the incident shock wave and substantially reduce the blast-pressure leakage into the building. On the other hand, the safety valve should exhibit a low pressure drop in normal operation in order to reduce the power consumption of the ventilators. One main difficulty in the design of such safety valves is to meet the minimum technical requirements, while ensuring the functionality in intrinsically different operating modes. Therefore, the present study proposes a target-oriented evaluation and optimization procedure for such devices, incorporating comprehensive numerical and experimental investigations. CFD, FEM and FSI analyses are regarded as an appropriate approach to predict valve performance parameters and to gain additional insights into the flow or structural behavior of the safety valve, which serves then as a basis for geometrical optimizations. The introduced procedure is exemplified on an existing passive air blast safety valve as a case study. The performance of the new design is significantly increased in ventilation operation, while meeting the performance criteria in the stress case when subjected to blast loads.

1. Introduction

The purpose of passive air blast safety valves is to protect people and technical installations in buildings or facilities. Typically, multiple safety valves are mounted in parallel on the building facade at the ventilation intake or exhaust. In case of explosions, e.g. due to technical failures in an oil- and gas refinery, the safety valve should substantially reduce the pass-through overpressure generated by the incident shock wave. A passive air blast safety valve must meet the following criteria: on the one hand, it should exhibit a low pressure drop in normal operation in order to reduce the power consumption of the ventilators. On the other hand, it should withstand the incoming blast load as well as close in milliseconds with the incident shock wave and reopen when the overpressure decreases to ensure the functionality of the ventilation after the impact. One main difficulty in the design of such safety valves is to meet the minimum technical requirements while ensuring the functionality in intrinsically different operating modes. An optimized safety valve concerning pressure drop in normal operation does not necessarily meet the minimum specifications in the stress case and vice versa. Consequently, several studies handle the topic of blast waves and their impact effects.

Shock tube experiments and computational fluid dynamics (CFD) simulations have been widely applied to investigate the generation and behavior of shock waves as well as to determine the high speed flow characteristics of different working fluids at different boundary conditions (Kumar and Nedungadi, 2020; Singh et al., 2020; Khawaja et al., 2016; Kim et al., 2017; Rigas and Sklavounos, 2005). As an example, Kumar et al. conducted a comprehensive CFD study to determine the effects of various design parameters (i.e. membrane burst pressure, driven section length and driver gas) of an open shock tube with respect to the generated pressure wave (Kumar and Nedungadi, 2020). Among other findings, it was discovered that high membrane burst pressures do not influence the decay rate of pressure waves, where however the driver gas has a significant effect on the blast wave shape. Another study evaluated three differently sized membranes (separation of the driver and driven section in the shock tube) in order to determine the maximum incident energy at the shock tube end with an experimentally validated CFD simulation (Singh et al., 2020).

* Corresponding author.
E-mail address: frank.tillenkamp@zhaw.ch (F. Tillenkamp).

https://doi.org/10.1016/j.jlp.2021.104706
Received 9 August 2021; Received in revised form 14 October 2021; Accepted 29 November 2021
Available online 18 December 2021

Nomenclature

Abbreviations

CFD	Computational fluid dynamics
DoE	Design of experiments
EN	European standard
FEM	Finite element method
FSI	Fluid structure interaction
GUM	Guide to the Expression of Uncertainty in Measurement
IEC	International Electrotechnical Commission
ISO	International Organization for Standardization

Variables

i	Shock wave impulse [bar ms]
L	Length [m]
$\dot{m}$	Mass flow rate [kg/s]
p	Pressure [Pa]
t	Time [s]
T	Temperature [K]
$\dot{V}$	Volume flow rate [m^3/h]
Δp	Pressure drop [Pa]
φ	Relative air humidity [%]

Subscripts

0	Initial
$close$	Closing
$crit$	Critical
DT	Driver tube/section
E	Entry
max	Maximum
$meas$	Measured
ML	Measuring location
res	Residual

Superscript

+	Positive pressure phase

An increase in incident energy was found with increasing membrane thickness, where the former yields approximately 47, 28 and 10 kJ with a diaphragm thickness of 4, 3 and 2 mm, respectively. Rigas et al. performed CFD simulations of an explosion with the corresponding shock wave propagation in a small scale tunnel configuration to determine the maximum overpressure and arrival time at different positions in the tunnel branches (Rigas and Sklavounos, 2005). The results are compared with experimental data, where the relative error of the peak overpressure and shock wave arrival time was found to be in a range of 7.5 to 18.2% and –16.7 to 4.5%, respectively. The authors conclude that CFD can be an effective tool to predict explosion hazards in confined complex geometries.

Besides the fluid mechanical characterization of shock waves (e.g. propagation, gas property changes, etc.), structural responses, caused by the impact of blast waves, are subject of several studies (Spranghers et al., 2013; Børvik et al., 2009; Henchie et al., 2014; Nguyen and Gatzhammer, 2015; Louar et al., 2015; Yang et al., 2013). Typically, experimental or numerical investigations are carried out, where for the latter finite element method (FEM) analyses or fluid structure interaction (FSI) simulations find application. In FEM analyses predefined load profiles are usually specified, where subsequently the structural response is simulated. The FSI modeling approach considers on the one hand the displacement or deformation of the investigated structure due to fluid forces (e.g. pressure), and on the other hand, the effects on the fluid flow behavior due to these structural movements. For example, Spranghers et al. analyzed the behavior of aluminum plates when exposed to planar blast waves in free air (Spranghers et al., 2013). In experiments, the plate deformation and the occurring reflected pressures were identified by two high-speed cameras with digital image correlation and pressure sensors in the mounting frame, respectively. The experimental results obtained are then compared with numerical FEM simulations, where different model parameters are investigated (e.g. element size and integration method). Consequently, a good agreement between the experimental and numerical results of the plastic deformation as well as the subsequent elastic vibrations of the plate is achieved. In another study the structural response of an unprotected ISO container under 4000 kg TNT blast loading at 120 m distance was investigated experimentally as well as numerically (Børvik et al., 2009). Different numerical approaches are applied for the analysis, where the coupled and uncoupled Eulerian–Lagrangian method resulted in a minor permanent structural deflection of the container wall compared to the measurements. Conversely, it is revealed that a purely Lagrangian analysis overpredicts the total deformation. However, the authors mentioned that according to the obtained measurement data, the reflected impulse was higher than applied in the simulations. By considering the correct blast load, the fully coupled approach delivers an adequate structural response compared to the experimental data. Henchie et al. accomplished experimental as well as numerical investigations to determine the behavior of circular plates when exposed to repeated uniform blast loads (Henchie et al., 2014). It was found that the plate midpoint deformation increases with each blast exposure for all different applied explosive charge masses. Furthermore, by comparing the numerical with experimental results, the determined impulses are mostly within an error band of ±10%, where all the predicted plate deflections lie in an error band of ±2–3 mm. Furthermore, Nguyen et al. investigated and proposed a coupling method for FSI simulations considering explosion blast waves and deformable structures (Nguyen and Gatzhammer, 2015). In one of the examined case studies, the blast load on an aluminum square plate and the corresponding center displacement was simulated, where good agreement with experimental data from another study was achieved.

Concerning passive air blast safety valves, Mo et al. conducted numerical investigations of a blast safety valve for pipeline systems with a translatory mode of operation (Mo et al., 2015). In normal operation, the movable valve core is held in place by a spring. When exposed to a shock wave, the spring is compressed and ultimately the valve core closes the flow passage. The CFD analysis revealed the expected pressure increase and reduction before and behind the safety valve during blast impact, respectively. Sharma et al. investigated numerically the behavior of hemispherical shells, which are typically present in many safety valve closure mechanisms, when subjected to blast loadings (Sharma et al., 2017). It is revealed that the radial displacement of such shells is minor compared to flat structures. The same authors conducted a literature review of existing blast safety valves and related studies (Sharma et al., 2016). A classification of existing safety valves is carried out, where it is among others differentiated between remote actuated (active) and blast actuated (passive) valves. It is mentioned that most of the available products on the market are designed for an incident pressure of 3 to 7 bar and having air volume flow rate capacities of 0.14 to 16.5 m^3/s. Furthermore, various related topics and concepts were addressed, e.g. blast wave behavior and impact as well as numerical modeling. The authors conclude, that the problem of blast pressure leakage in safety valves has not been thoroughly addressed in open literature and that FSI analyses of complete safety valves have not been carried out at that date. They mention the need of investigations, eventually incorporating FSI simulations, in order to optimally design air blast safety valves and to reduce the pass-through overpressure.

According to the literature search, several studies handle the topic of shock waves as well as air blast impact and the corresponding effects on different mechanical structures, where experimental and numerical methods are applied. However, to the best of the authors knowledge, only few publications handle specifically the topic of passive air blast safety valves. Therefore, the study proposes a target-oriented evaluation and optimization procedure for such devices considering both operating modes, i.e. ventilation operation (normal operation/case) as well as closing behavior when subjected to air blast loads (stress case). The goal is to investigate and reduce the pressure drop in normal operation as well as the blast pressure leakage of the valve in the stress case. This involves experimental as well as numerical investigations, where ultimately the introduced procedure is exemplified on an existing passive air blast safety valve as a case study.

2. Investigated system

In the present work the Andair AG passive explosion safety valve of type KC-T is investigated as a case study. It is a double acting, non-locking valve, i.e. it closes in positive as well as negative pressure phases during shock and reopens after the impact. The latter is important to assure the functionality of the ventilation system after the incident. The closing mechanism consists among others of aluminum bars and wire springs with a combined translational and rotational mode of operation, where however the translatory movement is dominant. The safety valve is designed for reflected shock wave pressures of up to 21 bar and is mostly applied for ventilation flow rates of 500 to 670 m^3/h. At the present date, there is an increased demand of safety valves for significantly lower expected incident blast wave pressures of 0.1 to 1 bar. For this field of application the mentioned valve is too expensive, massively oversized and therefore not optimal. Consequently, it is subject of optimizations or novel developments specifically for these shock wave magnitudes.

3. Experimental methods

3.1. Normal operation test rig

During the present work a new test rig is conceptualized for analyzing the passive safety valves in normal operation (see Fig. 1). It consists principally of four ventilators, two sections for mass flow rate measurements ($\dot{m}_1$ and $\dot{m}_2$) and two boxes, with the safety valve mounted in its middle. A deflection and perforated plate in the first box assures a uniform flow distribution, where the box entry pressure p_E, relative air humidity φ_E and temperature T_E are logged with corresponding measuring equipment. The pressure drop Δp over the valve is measured with a differential pressure gauge and a ring line around each box. The primary purpose of this new developed test rig is to fully characterize the behavior of the existing and novel safety valves in ventilation operation. Especially the pressure drop for given mass flow rates or vice versa is of main interest. Furthermore, the critical mass flow rate (closing point of the valves) can be determined likewise. Based on these requirements, a measuring concept is elaborated and an uncertainty analysis according to ISO/GUM is conducted (GUM, 2008). To ensure accurate results of the implemented measuring equipment, a calibration of each device is carried out by accredited calibration laboratories according to ISO/IEC 17025. Before the actual measurements, a validation procedure is carried out, to ensure the reproducibility and repeatability of the applied testing method. This novel concept provides reference values (i.e. pressure drop in function of the mass flow rate) for performance analysis between the existing and newly developed safety valves as well as data to validate the CFD models.

3.2. Shock tube test rig

As mentioned in the introduction, shock tubes are frequently used devices to generate and simulate shock waves. They comprise a high- and low-pressure section, often referred to as driver and driven section, separated by a diaphragm. Pressure waves are generated by abrupt burst of the latter, implying changes in fluid pressure, density, velocity and temperature. The incident shock wave generated in the shock tube depends from several design parameters such as driver gas and burst pressure.

For the present investigation of passive air blast safety valves in the stress case, a shock tube test rig at the SPIEZ LABORATORY is used (see Fig. 2). The test rig consists of a driver and a driven pipe section as well as a measuring section (if valves are assessed). Additionally, small discharge pipes to the environment in the driven and measuring section are present. Piezoelectric pressure sensors are mounted to monitor the incident and reflected pressures with respect to time in the shock tube. The driver gas is ambient air, where preliminary tests with an empty shock tube (see Fig. 2a) revealed a membrane burst pressure of 4.6 bar to generate an incident shock wave with a magnitude of approximately 1 bar. The latter represents the worst-case of the examined scenarios and is applied as boundary condition to test the existing as well as novel valve designs. For the experimental investigation of the valves, they are flanged at the end of the driven section (see Fig. 3), where a measuring pipe section is mounted thereafter (see Fig. 2b). With an additional pressure sensor, the blast pressure leakage through the valve as well as the closing time is measured. Again, the measurement data may be used to validate the numerical models.

4. Numerical methods

4.1. CFD

The commercial code ANSYS CFX 18.2 is used in the present study for the CFD analysis. Details of the code are provided in the appropriate handbooks of the software (CFX, 2017), where the most relevant information is given here. The governing equations (conservation of mass, momentum and energy) are spatial discretized to formally second order accuracy, in a finite volume formulation using structured meshes. Additionally, the solver employs a fully implicit approach for time discretization. The fully discretized system of linear equations are solved using an iterative technique. Sub-, trans- and supersonic flows can be modeled when compressible fluid models are used with either ideal or real gas laws. In the present case, the ideal gas law is applied. For temperature calculations in the solution domain a heat transfer model (total energy formulation) is applied, to account for kinetic energy effects. Turbulence is accounted for by the BSL or SST model (Menter, 1994), since they has been shown to reliably capture flow separation in various applications (CFX, 2017).

For both operating modes of the safety valve, the fluid domain is modeled as close as possible to the real situation in the mentioned test rigs (compare Section 3). To reduce the computation time, components with a minor effect on the fluid flow, e.g. mounting screws, are neglected. For the normal operation, the two boxes of the test rig with the flanged safety valve are modeled. A uniform flow distribution is assumed at the inlet, where mass flow rates according to the measurements are specified. The walls are defined as a no-slip wall boundary condition and a relative pressure of 0 Pa is specified at the outlet. For the simulation of the stress case, the whole shock tube (except the discharge pipes) is modeled, where no-slip wall boundary conditions and a relative pressure of 0 Pa at the discharge pipe junction is defined. The pressure initial conditions are specified according to the empty shock tube measurements (4.6 and 0 bar in the driver and driven section, respectively), which generates a 1 bar incident pressure wave. The structured computation grid for all simulations is generated with ANSYS ICEM CFD 18.2, where mesh independence studies are carried out to minimize eventual discretization errors (see Appendix A).

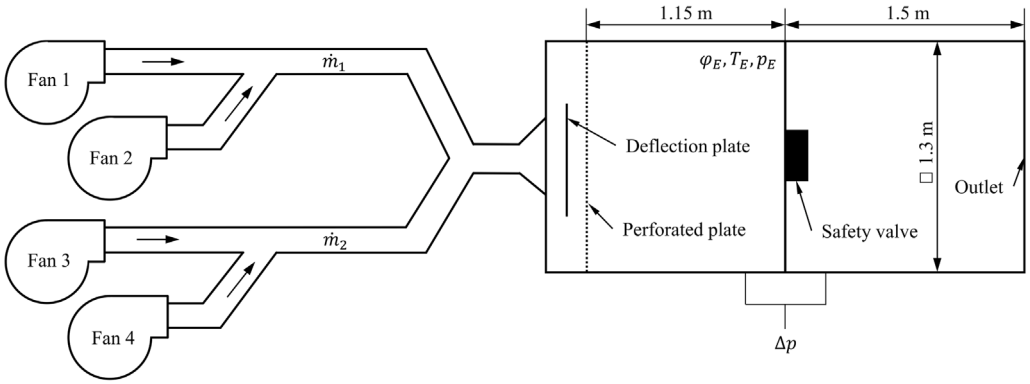

Fig. 1. Schematic of the normal operation test rig with the essential components, dimensions and measuring locations (not true to scale).

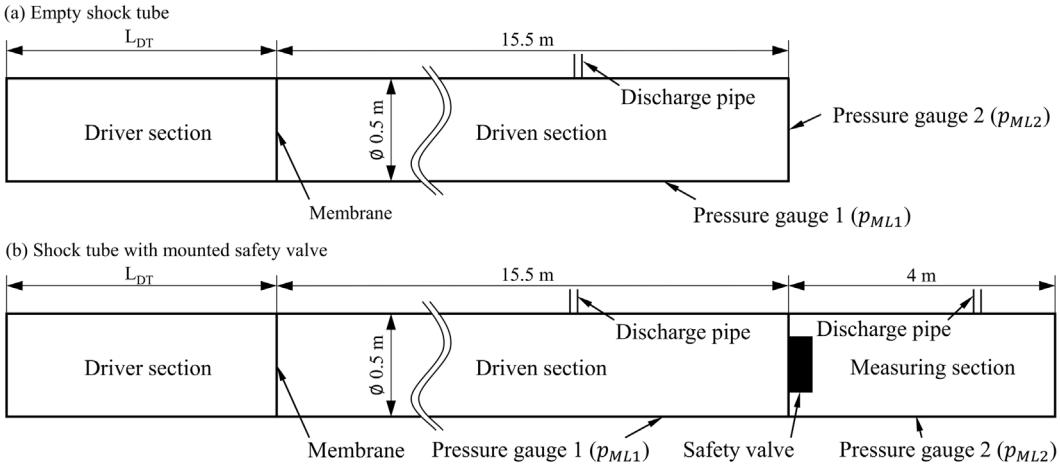

Fig. 2. Schematic of the shock tube with the essential components, dimensions and measuring locations (not true to scale): (a) emtpy shock tube configuration and (b) safety valve measurement configuration.

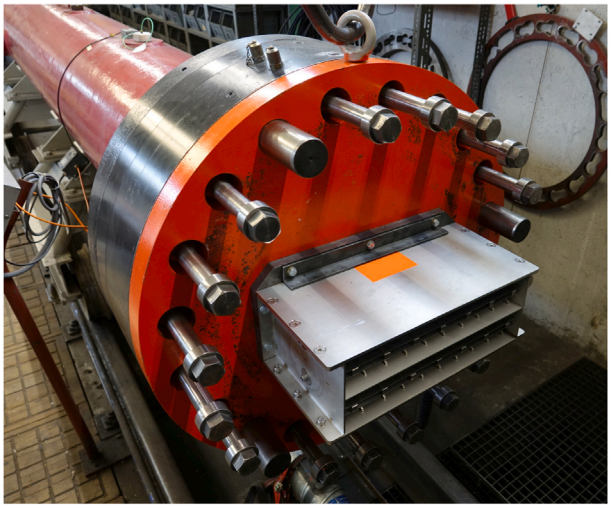

Fig. 3. Photograph of a flanged safety valve at the end of the driven section in the shock tube (without measuring section).

4.2. FEM

Structural simulations of valves during stress situation are performed using ABAQUS/CAE, Version 2018. A detailed description of the code is available in the ABAQUS Theory Guide (Aba, 2018). In dynamic analysis an implicit scheme for time integration is used, with automatic time-stepping based on the concept of half-increment residuals. Spatial discretization is implemented with structured meshes of linear order. Contact pairs are discretized using a true surface-to-surface discretization. The discretized equations are iteratively solved in their weak formulations.

Individual parts are constrained in accordance with the real situation. Materials of components subjected to large deformation are modeled using an elastic–plastic bilinear model based on available material data acquired according to EN 10151. The blast wave loads are specified as boundary conditions by importing pressure–time curves based on the CFD shock tube simulations, assuming a uniform pressure-distribution over the entire valve.

4.3. FSI

In theory different numerical approaches exist for FSI simulations. With the so called monolithic approach, fluid and solid mechanics governing equations are solved simultaneously. Conversely, in the partitioned approach, the fluid and solid domain are separated numerically and the governing equations are solved individually in an iterative procedure (Ha et al., 2017). In the latter approach, it can be further distinguished between one- and two-way coupling. With one-way coupling, only fluid pressure forces are transferred via an interface to the structural solver at every time step, where the structural deflection is computed subsequently. This approach is usually applied if the structural response has a minor effect of the fluid flow characteristics. With two-way coupling, the structural deformation and displacement is additionally imported to the fluid solver at every time step and the

computation domain is adapted accordingly (Benra et al., 2011). This full coupling becomes especially important in the case of blast safety valves, where the closing mechanism has a significant effect on the fluid flow. Different studies cover the topic of FSI simulations considering blast wave loads and highly deforming geometries or structural failure (Yuan et al., 2017; Subramaniam et al., 2009; Faucher et al., 2019; Kambouchev et al., 2007). For example, Yuan et al. evaluated the behavior of a clamped ductile beam with large elasto-plastic deflection when subjected to an underwater blast applying an analytical FSI framework (Yuan et al., 2017). In another study, a numerical method for FSI analysis and an approach to determine its influence on the structural response parameters is introduced (Subramaniam et al., 2009).

Consequently, a two-way coupling approach is considered in the present work. Due to numerical issues and interface mapping problems, it was not possible to solve directly the fluid flow and structural response iteratively at every time step. Therefore, a so-called indirect two-way coupling is applied. Meaning, that time-dependent pressure forces evaluated from the complete CFD simulation (i.e. the whole blast load period) are transferred to the FEM analysis, where the displacement and deformation of the valve closing mechanism is calculated. The determined time-dependent deflection is then used as a new boundary condition for the next CFD simulation. Several iterations of the indirect coupling are carried out, until the change of the time-varying pressure curve was insignificant. Based on the dominant translational motion of the existing closing mechanism, the immersed solid capability (overset mesh method) of ANSYS CFX is applied. This method allows a motion of solid bodies through fluid domains and thus fully closing the safety valve in the CFD simulation. However, for some novel valve designs, the immersed solid strategy cannot be used due to mixed modes of operation (e.g. closing mechanism based on rotation and material deformation). Alternatively, a mesh morphing strategy is adopted, were the position of the valve closing mechanism is iteratively adapted in the CFD computation with respect to the determined displacement characteristics of the whole blast load period by FEM analysis. However, with this method the valve closure cannot be modeled completely in the CFD simulation due to mesh deformation issues. Nevertheless, such indirect FSI simulations yield first important insights concerning the valve performance when subjected to shock wave loads, which serve as a basis for geometrical optimizations.

5. Valve performance evaluation criteria

To compare the performance of the existing valve concept with novel ones, adequate evaluation criteria need to be specified. In ventilation operation, the pressure drop Δp with respect to the present volume $\dot{V}$ or mass flow rate $\dot{m}$ is applied for the evaluation in the present work. A decrease in pressure drop at the same given volume flow rate represents a valve performance enhancement (compare schematically Fig. 4a). $\dot{V}_{crit}$ represents the critical volume flow rate, at which the valve closes in normal operation.

In the stress case, the maximum overpressure p_{max} behind the valve and the valve closing time t_{close} (i.e. when the relative pressure reaches zero) during the shock wave impact is of relevance. To quantify the total blast pressure leakage, i.e. the strength of the shock behind the safety valve, the residual impulse i_{res} is applied as a performance criterion, which graphically represents the area below the positive pressure phase after the safety valve until its closure. Next to the maximum overpressure, this quantity is important to estimate the damage potential on structures, devices or personal injuries (Malhotra et al., 2017; Zalosh, 2014). The residual impulse i_{res} is defined as:

$$i_{res} = \int_{t_0}^{t_{close}} p(t)\mathrm{d}t \tag{1}$$

with t_0 the initial time of pressure increase, t_{close} the closing time of the valve (i.e. when the overpressure behind the valve reaches 0 Pa) and $p(t)$ the temporal pressure distribution behind the safety valve after shock wave impact. A decrease of all mentioned quantities represents a valve performance increase, i.e. a reduction of shock strength behind the valve (compare schematically Fig. 4b). However, a low maximum overpressure not necessarily results in a low residual impulse, if the closing time of the valve is elevated. In the present work limiting values of i_{res} and p_{max} of 1.5 bar ms and 1 bar, respectively, are specified for the shock wave downstream of the safety valve. Values above would most likely cause damage to technical components and installations.

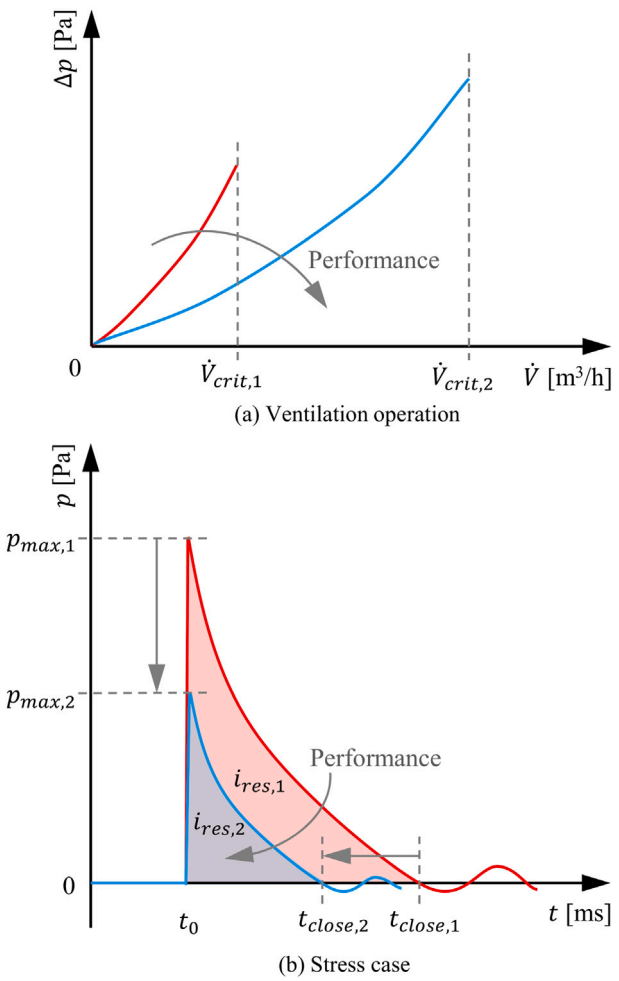

Fig. 4. Schematic representation of the different applied evaluation criteria for passive air blast safety valves in (a) ventilation operation and (b) stress case. Arrows indicate the direction of performance increase.

6. Evaluation and optimization procedure

Fig. 5 shows a flow chart of the proposed evaluation and optimization procedure. With the presented set of experimental and numerical methods as well as evaluation criteria, the existing safety valve is first assessed in normal operation. On the purpose-built test rig, the pressure drop is determined at various air volume flow rates ranging from approximately 200 to 800 m³/h. To fully characterize the fluid flow behavior in the safety valve and to gain further in-depth insights, the same operating points and the corresponding pressure losses are analyzed with CFD simulations. Moreover, the existing valve is assessed experimentally in the shock tube with an incident pressure wave of 1 bar, where the blast pressure leakage is analyzed. The maximum overpressure, closing time as well as the residual impulse is determined. Simultaneously, FSI analyses are set up to simulate the valve closing behavior and to determine the fluid flow characteristics behind the safety

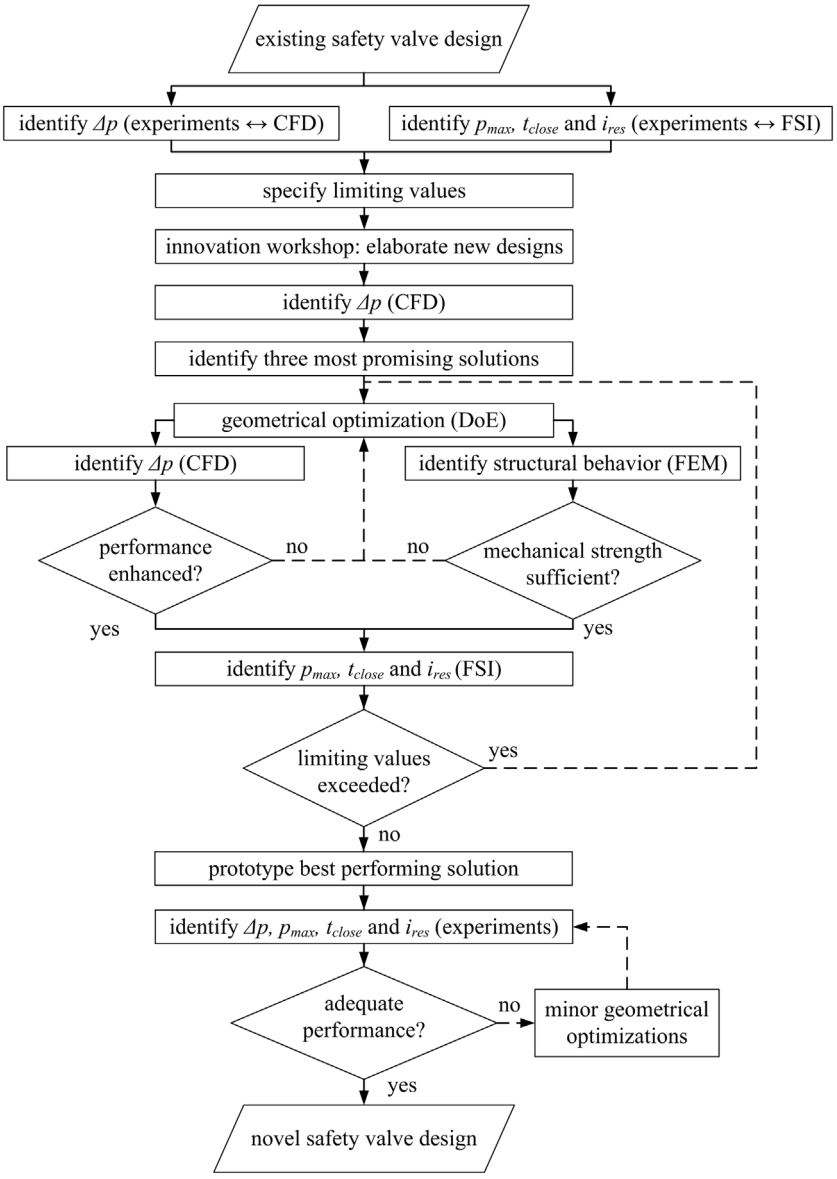

Fig. 5. Flow chart of the evaluation and optimization procedure for passive air blast safety valves incorporating experimental and numerical investigations.

valve. From the obtained experimental and numerical results, reference values based on the evaluation criteria (e.g. pressure drop, residual impulse, etc.) are defined next to the limiting values as baseline for the further development and the comparison with novel valve designs. Also, the measurement data is applied to validate the numerical models if possible, in order to assure their applicability for the upcoming optimization investigations.

After the characterization of the present system and based on the gained knowledge, novel valve concepts are elaborated in an innovation workshop. All variants are assessed with CFD analysis in ventilation operation to determine the respective pressure losses. The three most promising solutions are further optimized regarding pressure drop with the design of experiments (DoE) method. At the same time, CFD and FEM analyses are carried out to gain first indications regarding the valve closing behavior when subjected to blast loads as well as to assess the structural response, e.g. if the mechanical strength of the design is sufficient. In an iterative procedure both variants are geometrically optimized with respect to the defined reference and limiting values as well as technical requirements. Subsequently, a prototype of the best performing solution according to the numerical investigations is manufactured and assessed experimentally. First, the valve is examined on the normal operation test rig to determine the pressure losses as well as the limiting mass flow rate and the corresponding valve closing characteristics. The latter gives first indications for the behavior in the stress case, which is assessed subsequently on the shock tube. Additionally, the normal operation performance of the safety valve after blast wave impact is determined to assure its functionality after an incident. In the end, after minor geometrical optimizations determined by simulations and experiments, the final design of the novel passive air blast safety valve is elaborated.

7. Results and discussion

7.1. Novel valve design

Fig. 6 compares the existing with the novel passive air blast safety valve design resulting from the optimization procedure. Like the existing design, the new one has a double acting and non-locking mechanism, which closes in positive as well as negative pressure phases during shock and reopens after the impact. The closing mechanism consists of metal sheets, which spread open under blast load (see Fig. 6b). To prevent these sheets from folding over under blast load as

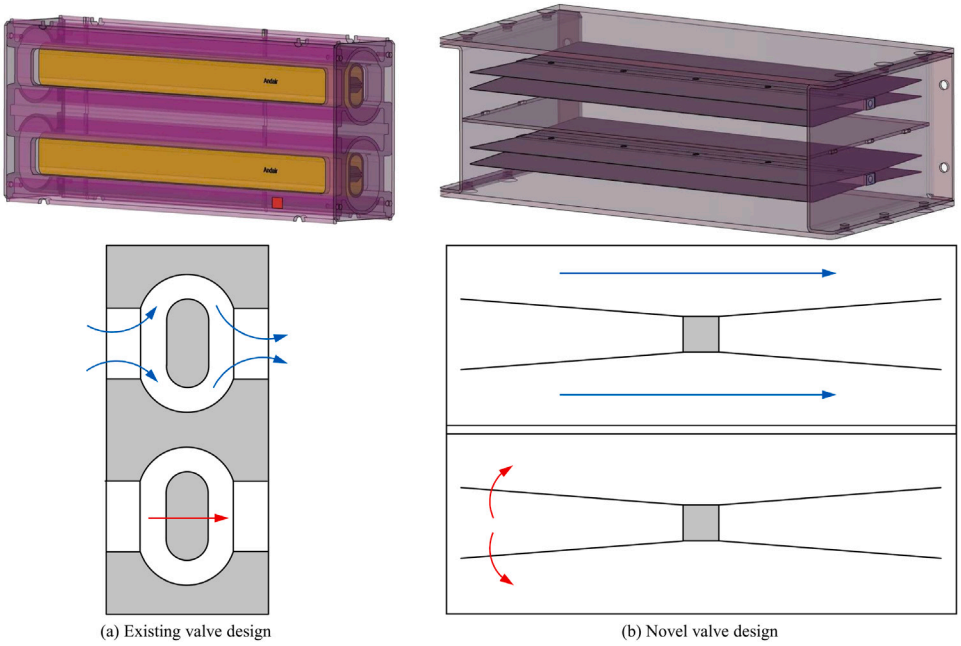

Fig. 6. 3D representation and simplified schematic of the different passive air blast safety valves: (a) existing and (b) novel design. Blue and red arrows indicate the air flow path and closing mechanism behavior, respectively. (For interpretation of the references to color in this figure legend, the reader is referred to the web version of this article.)

well as to reduce vibrations in normal operation, additional supports are installed. Therefore, the closing mechanism reveals a mixed mode of operation, which bases on rotational movement as well as elastic material deformation. In comparison to the existing valve, the new design has an increased air flow cross section and a significantly reduced mass of the closing component. Consequently, a reduced pressure drop in normal operation as well as a reduced closing time in the stress case are to be expected.

7.2. Ventilation operation

Fig. 7 shows the pressure drop Δp (y-axis) of both valve designs in function of the volume flow rate $\dot{V}$ (x-axis). Symbols indicate the measured as well as simulated pressure losses at specific flow rates, where the dashed and dotted lines reveal the valve behavior approximated with a power-law fit based on the acquired data. Fig. 8 depicts a velocity contour plot from CFD analysis in a vertical cut through the valves at a volume flow rate of 791 m^3/h.

First of all, the novel valve concept reveals a significant performance increase in ventilation operation (see Fig. 7). At a pressure drop of 200 Pa, the throughput is increased by approximately a factor of 3 from 673 to 2000 m^3/h. When evaluating the pressure loss at a volume flow rate of 791 m^3/h, the novel valve design yields a value of approximately 32 Pa in comparison to 314 Pa of the existing valve. The reason for this behavior is most likely the increased flow cross section as well as the straightened flow path in the new valve design. Also, this outcome is of relevance in practice, since this design may helps to reduce the power consumption of ventilation fans or requires a decreased number of valves installed in the building facade, without being critical for the ventilation operation.

When examining the velocity contour plot of the CFD analysis (see Fig. 8), it is revealed that the maximum flow speed in the new safety valve design is reduced by approximately 21.2 m/s in comparison to the existing concept at the same given volume flow rate of 791 m^3/h. As suspected this is due to the straight air flow path and the increased flow cross section. Furthermore, the air flow in the novel design is close to steady state where the largest flow separation occurs mainly at the inlet (see Fig. 8b). Conversely, the existing design reveals a non-stationary behavior of the flow, where multiple regions with boundary layer separation are present due to the increased flow deflection (see Fig. 8a). Shedding vortices are observed after the closing bar and at the valve outlet (regions with velocities close to zero), which results in an increased pressure drag and a Kármán vortex street like flow behavior. Both phenomena contribute to the discovered increased pressure losses in the existing valve concept.

Moreover, the predicted pressure losses by CFD analysis fits qualitatively well the experimental data (see Fig. 7). The mean absolute error (MAE) is 15.9 and 5.7 Pa when comparing the numerical with the experimental data of the existing and the new valve concept, respectively. Therefore, the CFD model can be validated and the results demonstrate the usability of such analysis for the presented optimization procedure. With both variants, the absolute error grows with increasing volume flow rate and reaches its maximum of 24.9 (existing valve) and 16.7 Pa (new design) at the highest flow rate examined. Also, the CFD model predicts slightly lower pressure drop values in comparison to the measurements. On the one hand this can be explained by omitted components (e.g. mounting screws) in the analysis and on the other hand by assuming a fixed closing mechanism. The latter closes slightly in reality at higher volume flow rates, inducing a decreased flow cross section, which results in increased air flow velocities and pressure losses.

7.3. Stress case

7.3.1. Empty shock tube

Fig. 9 depicts the measured and simulated overpressure p (left y-axis) as well as positive phase impulse i^+ (right y-axis) in function of time t (x-axis) at both measuring locations (ML1 and ML2) in the empty shock tube (compare Fig. 2a). Solid and dashed lines represent the experimental and numerical results, respectively.

When considering the measured pressure–time distribution at measuring location 1 (see Fig. 9a), a first pressure increase of approximately 1.1 bar is visible until 7.5 ms due to the incident shock wave traveling towards the shock tube end flange. Subsequently, the pressure increases further by approximately 2.05 bar due to the reflected shock wave traveling backwards in the driven section. The overpressure starts to decrease at approximately 12 ms until reaching a value close to zero at 80 ms. Correspondingly, the impulse increases continuously

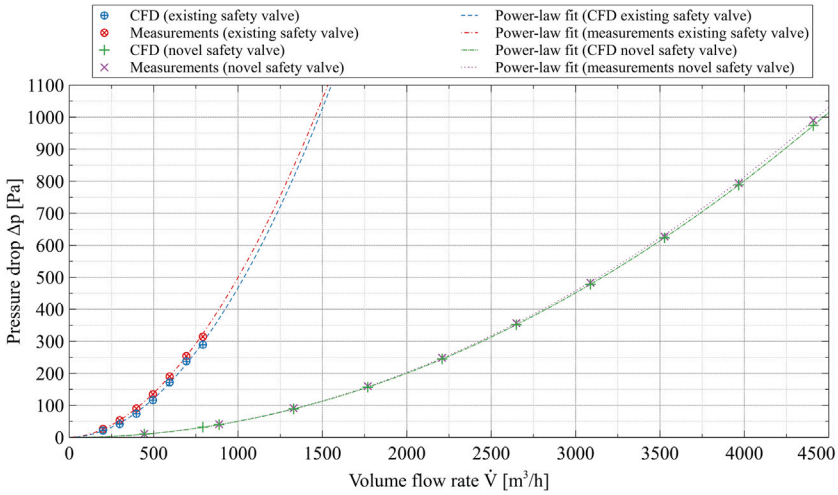

Fig. 7. Measured and simulated pressure drop in ventilation operation of the existing and novel valve design.

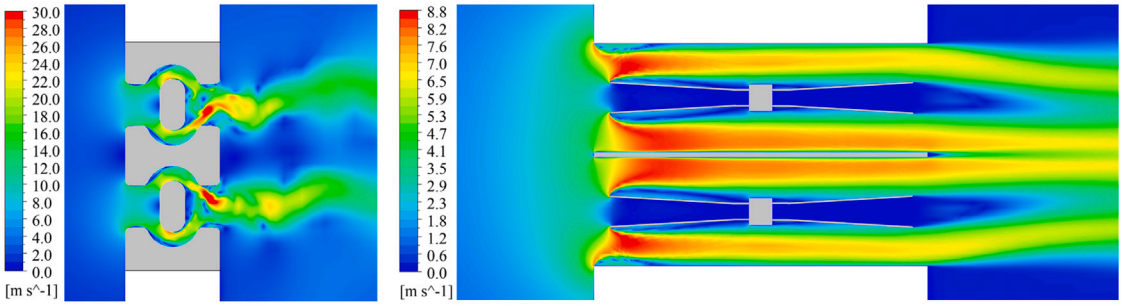

Fig. 8. Velocity contour plots at a volume flow rate of 791 m^3/h during ventilation operation in a vertical cut through the safety valves: (a) existing and (b) novel valve design.

until reaching a value of 86 bar ms over the whole positive pressure phase. The measured overpressure at the driven section end flange (see Fig. 9b) represents the reflected pressure, where 3.15 bar is reached on average. The pressure remains at the same level for approximately 12 ms, where a decrease is observed thereafter and a total impulse of 89 bar ms is reached. Initially, the experimental data fluctuates strongly in a range of up to 2.8 bar, where subsequently the amplitude decreases to approximately 0.15 bar. These fluctuations are also observed at measuring location 1, although much smaller, most probably induced by vibrations in the mechanical structure due to the incident shock wave.

Moreover, the simulated values show adequate agreement in general with the experimental data at both measuring locations (see Fig. 9). No significant fluctuations are present, except directly after the shock. The mean absolute error between the predicted and measured overpressure is 0.10 and 0.12 bar at measuring location 1 and 2, respectively. However, an underprediction of the pressure between 40 and 70 ms is observed. This results in slightly lower simulated positive phase impulse values of approximately 81.5 and 87 bar ms, where a mean absolute error of 1.46 and 1.68 bar ms is present. These errors are assumed negligible, since the high pressure phase in the beginning is of particular interest when evaluating the closing behavior of the valve designs. Consequently, the CFD analysis can be applied to accurately predict the blast load on the safety valves.

7.3.2. Safety valve performance

The present section reveals the safety valve performance and behavior when subjected to a blast load of approximately 1 and 3 bar incident and reflected pressure (as shown in Fig. 9), respectively. Fig. 10 depicts the measured and simulated overpressure p (left y-axis) as well as residual impulse i_{res} (right y-axis) after the valve at measuring location 2 (ML2) in function of time t (x-axis) of both designs. Solid and dashed lines represent the experimental and numerical results, respectively. In order to facilitate the comparison between the different valve designs and to assure a uniform benchmark, the performance criteria are evaluated when the residual pressure reaches 0 Pa for the first time. Furthermore, details of the flow field in the safety valves during blast loading are presented in Appendix B.

First of all, the existing valve design reveals a maximum measured overpressure of 0.55 bar and closes after approximately 2.25 ms (see Fig. 10a). This behavior results in a residual impulse of 0.39 bar ms until closure. This demonstrates an adequate performance of the valve, since the specified limiting values are not exceeded (compare Section 5). When considering the numerical results of the FSI simulation, an underprediction of the maximum overpressure by 0.18 bar as well as an overprediction of the closing time by 0.9 ms is visible. Due to the increased closing time and the slightly higher simulated pressures in the second half of the valve closing phase, an increased residual impulse of approximately 0.54 bar ms is observed. Possible reasons for this deviation from the experimental data are an inaccurate prediction of the flow field by the CFD analysis in the valve due to the applied geometrical simplifications or too stiff spring models in the FEM analysis. Nevertheless, the FSI simulation delivers important insights regarding the valve performance for geometrical optimizations, by means of a conservative estimate. It is assumed that if the limiting values are not exceeded in the simulation, the same applies for the real situation. This assumption can be verified when evaluating the blast load behavior of the novel valve concept.

With the new safety valve, the measured maximum overpressure is increased by 0.1 bar in comparison to the existing design and

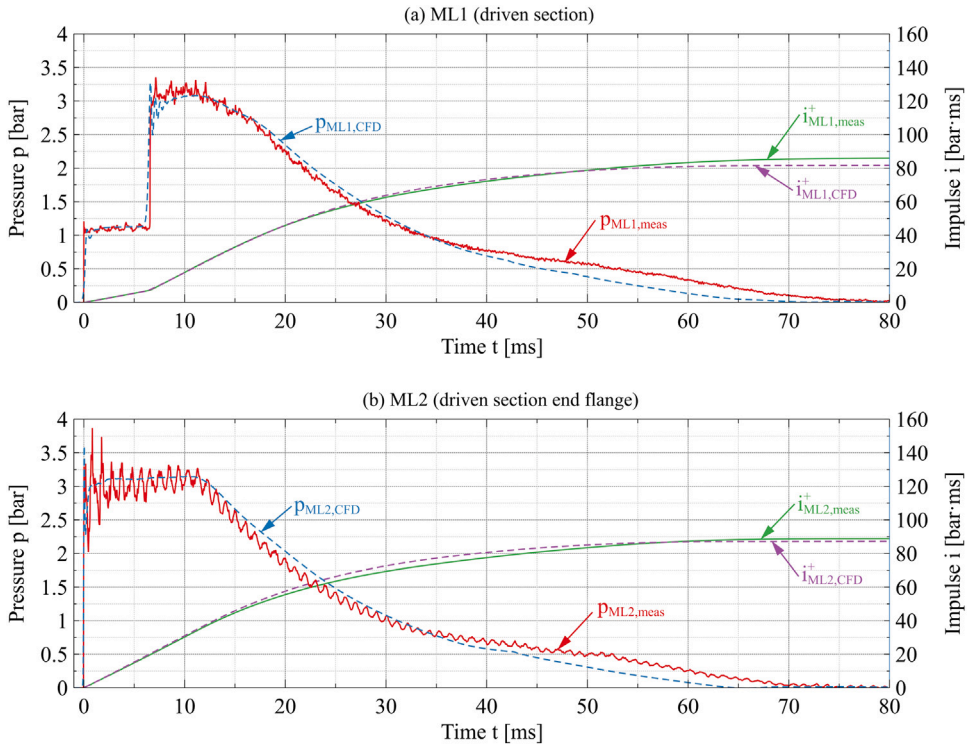

Fig. 9. Measured and simulated pressure–time distribution as well as positive pressure phase impulse: (a) measuring location 1 in the driven section, (b) measuring location 2 in the driven section end flange (compare Fig. 2a).

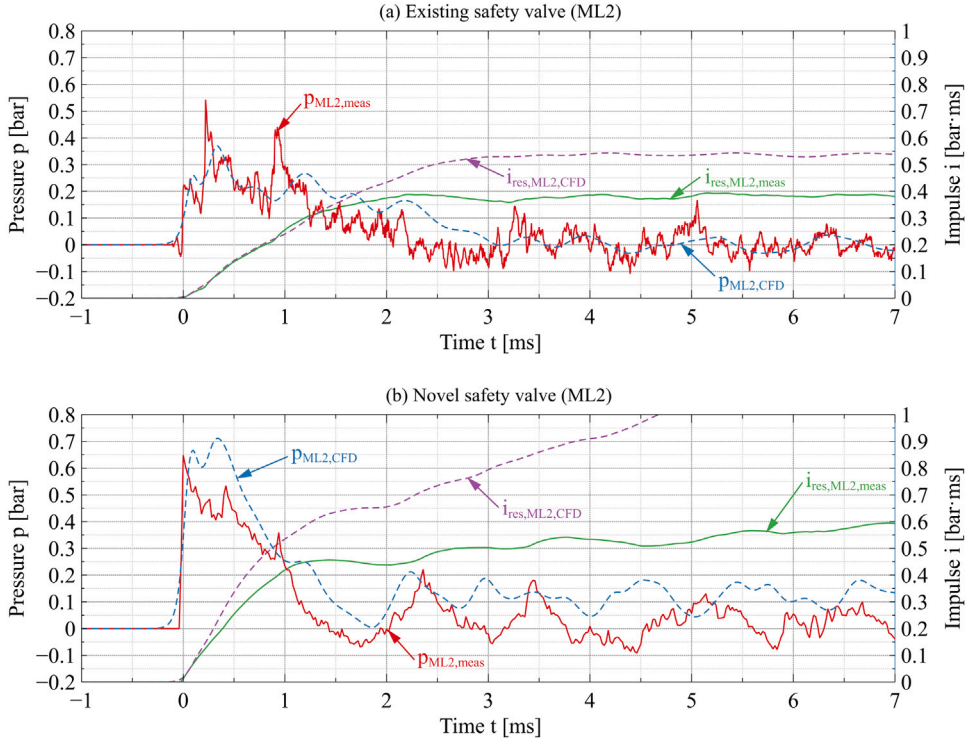

Fig. 10. Measured and simulated pressure–time distribution as well as residual impulse after the passive air blast safety valve (measuring location 2, compare Fig. 2b): (a) existing and (b) novel valve design.

reaches a value of 0.65 bar (see Fig. 10b). Conversely, the closing time is reduced by approximately 0.8 ms down to a value of 1.45 ms. Most likely, this behavior is due to the increased flow cross section (i.e. initially an increased amount of air passes through the valve) as well as the reduced mass of the closing mechanism components. The residual impulse reaches a value of approximately 0.45 bar ms until closure, which is roughly 30% of the specified limiting value. Therefore, the new safety valve concept reveals a similar performance under blast loading compared to the existing design. However, as shown in Section 7.2, the pressure drop in ventilation operation is significantly

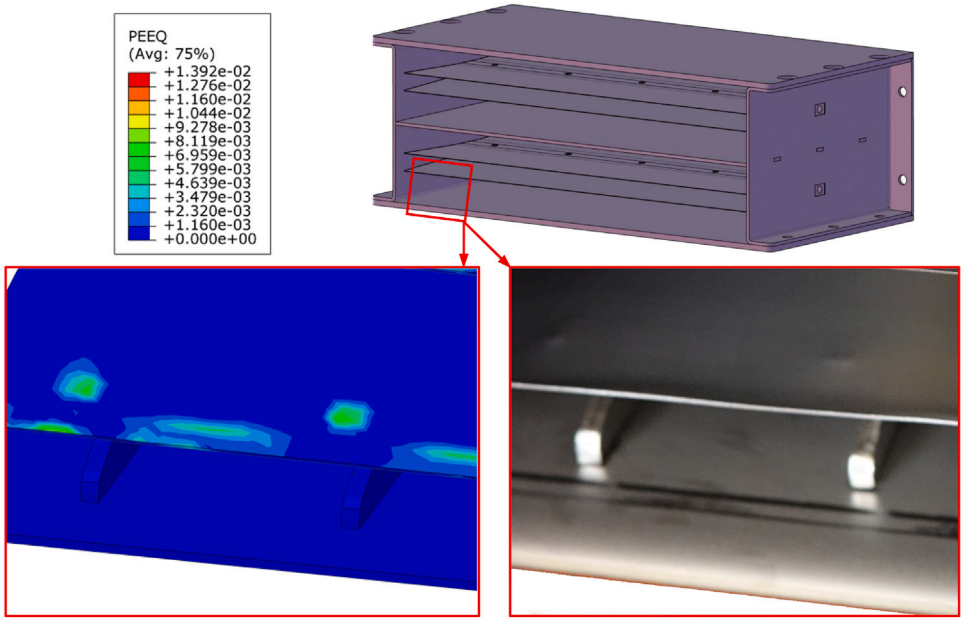

(a) FEM simulation (equivalent plastic strains) (b) Closing mechanism after shock wave exposure

Fig. 11. Comparison between (a) predicted and (b) observed plastic deformation of the metal sheet in the safety valve after shock wave exposure.

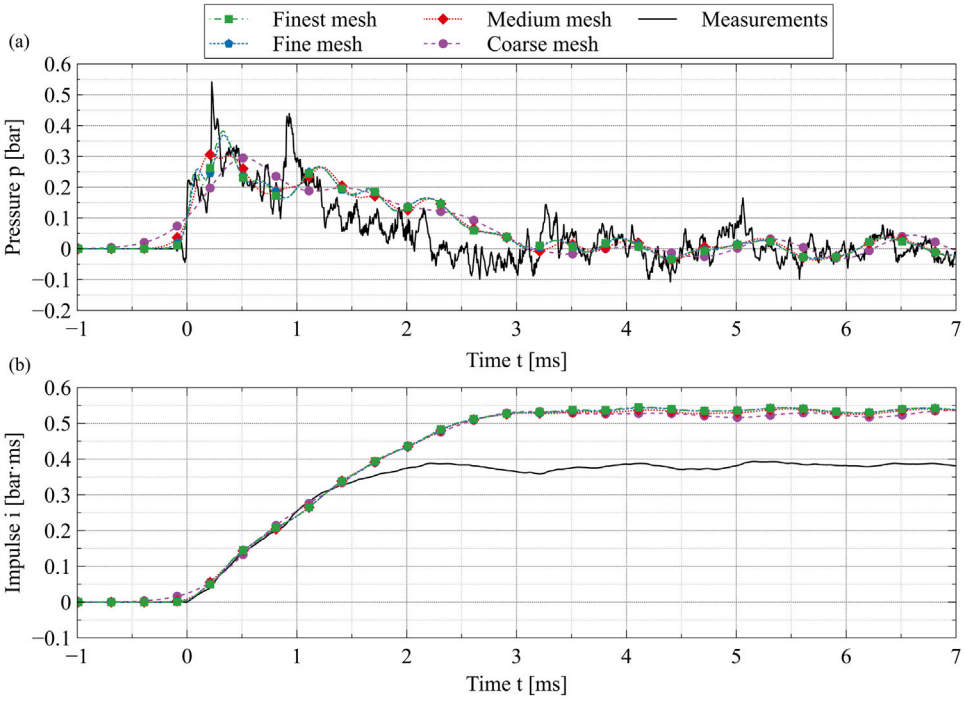

Fig. A.12. Results of the grid convergence study examined at measuring location 2 (compare Fig. 2b) after the existing passive air blast safety valve: measured and simulated (a) pressure as well as (b) residual impulse.

decreased. The pressure–time distribution of the FSI analysis shows a similar form in comparison to the measurements, where the maximum overpressure is slightly higher (≈0.7 bar) and a shift on the x-axis of approximately 0.5 ms is visible until the simulated valve closure at 1.9 ms. Subsequently, the pressure increases again and fluctuates around 0.1 bar. This is why the residual impulse reaches first a value of 0.65 bar ms and then continues to increase. As mentioned in Section 4.3, this behavior is induced by mesh deformation issues, where the valve cannot be fully closed in the simulation. This results in a continuous air flow through the valve during blast impact, which is observed by the pressure distribution above zero. Despite this fact, the FSI simulation provides a conservative estimate of the blast pressure leakage which is to be expected in reality.

It is also worth mentioning, that the FEM simulations yield an accurate estimation regarding the structural response of the new closing mechanism. Fig. 11 shows exemplarily an investigated section of the latter in the bottom left corner of the valve. For example, the equivalent plastic strains (PEEQ) were analyzed to estimate the plastic deformation of the metal sheets, and thus the potential occurrence of cracks within the sheets (see Fig. 11a). The predicted plastic deformations are confirmed by the prototype after the experimental shock tube tests (see Fig. 11b). In addition, the simulated closing behavior corresponds well

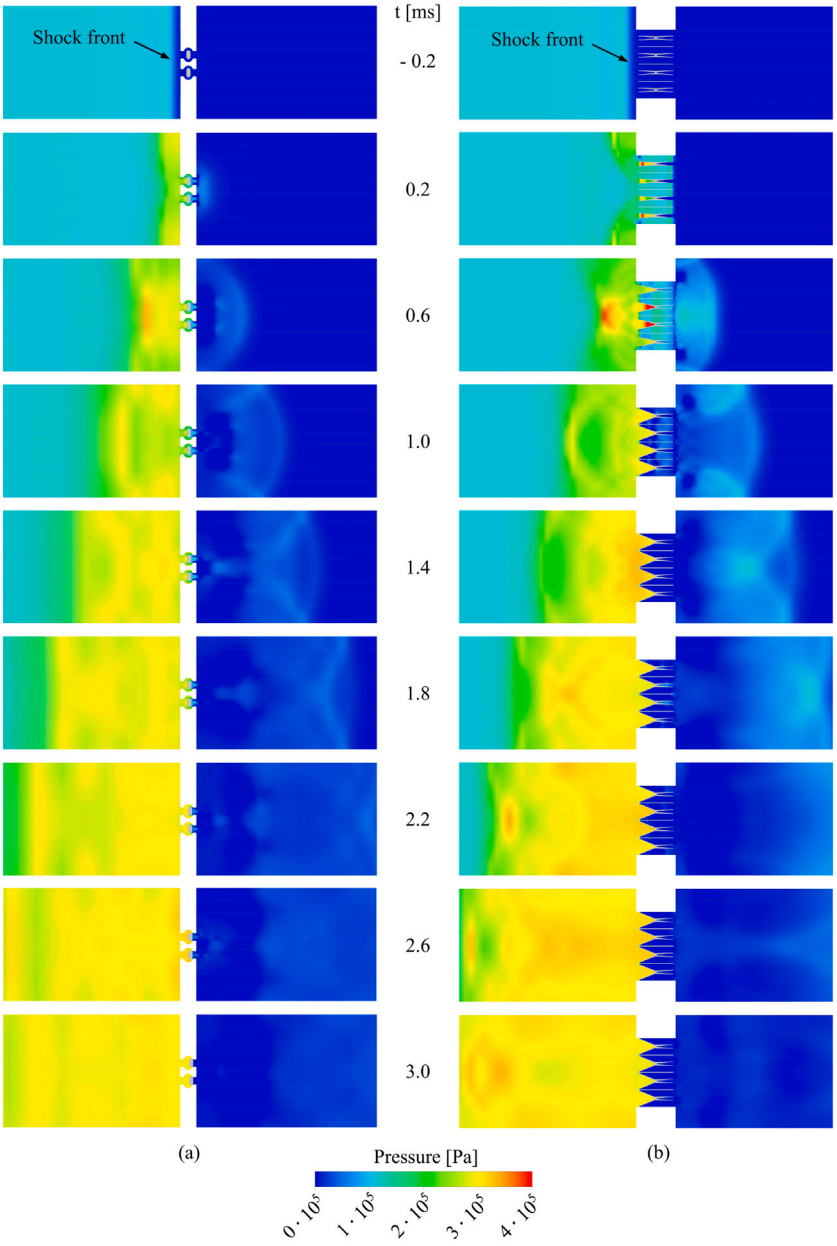

Fig. B.13. Pressure contour plot in a vertical cut through the safety valves and shock tube during blast loading at different time steps (fluid domain and closing mechanisms are shown): (a) existing and (b) novel valve design.

to the actual situation. If not, larger deviations in the pressure–time curve compared to the measurements would be visible.

8. Conclusion and outlook

The present study handles the topic of pressure drop and blast pressure leakage of passive air blast safety valves. An evaluation and optimization procedure for such devices is introduced, which incorporates comprehensive experimental as well as numerical investigations. To the best of the authors knowledge, the proposed method allows a target-oriented improvement of safety valves considering two intrinsically different operating modes: ventilation operation and the stress case when subjected to shock wave loads. Numerical analyses are regarded as an appropriate approach in order to predict valve performance parameters as well as to gain in-depth insights into the flow or structural behavior, which then serves as a basis for geometrical optimizations. Ultimately, the procedure is exemplified on an existing passive air blast safety valve as a case study.

Both, the existing and new safety valve design, reveal an adequate behavior when subjected to a blast load of 3 bar reflected pressure, which is the worst-case scenario for the contemplated application. Additionally, while not explicitly shown in the manuscript, the novel safety valve has been successfully tested experimentally for incident (reflected) pressures of 0.1 bar (0.2 bar) up to the presented worst-case. The obtained maximum overpressure and residual impulse are for both concepts up to a factor 1.8 and 3 lower than the specified limiting values of 1 bar and 1.5 bar ms, respectively. Furthermore, a significant performance increase of the novel valve design in ventilation operation is achieved. The volume flow rate is enhanced by a factor of 3 in comparison to the existing device, while the same pressure drop of 200 Pa is present. This outcome is of importance in practice, since it may allow to reduce the power consumption of the ventilation fans or requires less safety valves installed in the system.

Future work could cover the investigation of different air blast loads or other protective components with the shown method. Also, different

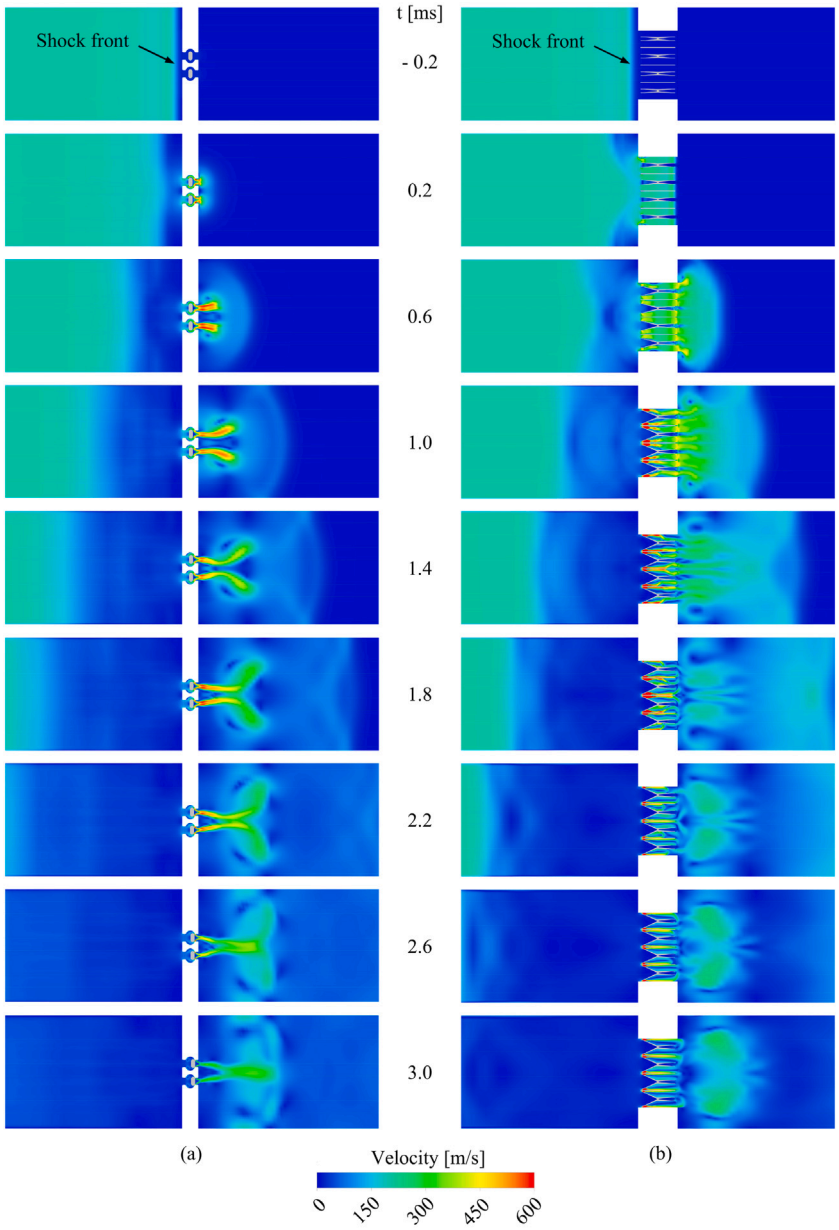

Fig. B.14. Velocity contour plot in a vertical cut through the safety valves and shock tube during blast loading at different time steps (fluid domain and closing mechanisms are shown): (a) existing and (b) novel valve design.

FSI techniques should be analyzed to simulate the valve behavior under blast loading. While the chosen indirect coupling approach delivers first important insights, there is room for improvements. Possibly, a direct two-way coupling approach would deliver more accurate results, which is however regarded as very challenging to achieve in short-term dynamic applications.

CRediT authorship contribution statement

Lorenz Brenner: Methodology, Formal analysis, Investigation, Writing – original draft, Writing – review & editing, Visualization. **Christian Jenni:** Methodology, Formal analysis, Investigation, Writing – original draft, Writing – review & editing, Visualization. **Flurin Guyer:** Methodology, Formal analysis, Investigation, Writing – original draft, Visualization. **Patrick Stähli:** Methodology, Software, Validation, Investigation, Writing – original draft, Visualization. **Robert Eberlein:** Conceptualization, Validation, Writing – review & editing, Supervision. **Matthias Huber:** Methodology, Formal analysis, Investigation, Writing – original draft, Visualization. **André Zahnd:** Validation, Writing – review & editing, Supervision. **Martin Schneider:** Validation, Project administration, Writing – review & editing, Funding acquisition. **Frank Tillenkamp:** Conceptualization, Validation, Writing – review & editing, Supervision, Funding acquisition.

Declaration of competing interest

The authors declare that they have no known competing financial interests or personal relationships that could have appeared to influence the work reported in this paper.

Acknowledgments

This study was funded by the Swiss Innovation Agency Innosuisse (grant no. 27913.1 PFIW-IW). The authors would like to thank Michael Riedo and Michel Schilling from Andair AG for providing test devices and for their in-depth technical knowledge of passive air blast

protection valves. Additionally, many thanks go to Angelo Seitz from SPIEZ LABORATORY and David Denzler from the Institute of Energy Systems and Fluid Engineering (IEFE) for their assistance throughout the experimental tests with the shock tube and the normal operation test rig, respectively.

Appendix A. Grid convergence study

Fig. A.12 shows exemplarily the behavior of the residual overpressure and impulse (y-axis) in function of the time (x-axis) of the existing safety valve design with different mesh resolutions. The average cell size ranges from 0.55 and 10 mm (finest mesh) to 1 and 40 mm (coarse mesh) when considering the safety valve and the shock tube, respectively. It is revealed that the pressure is more sensitive to the cell size compared to the impulse. Only the finer grids are able to approximately resolve larger intermediate peaks in the pressure–time history, e.g. the two distinguishable pressure increases during the first 0.5 ms (see Fig. A.12a). A pressure of 0 Pa is reached by all four computational grids at approximately 3.15 ms. The lowest and highest residual impulse compared to the measurements is reached by the coarsest and finest mesh, respectively (see Fig. A.12b). Qualitatively, no large deviation between the pressure–time histories of the finer grids is visible and the mean-relative error of the impulse is less than 1%. The fine mesh is therefore applied for the present investigations.

Appendix B. Safety valves flow field during blast loading

Figs. B.13 and B.14 show pressure and velocity contour plots in a vertical cut through the safety valves during blast loading at different time steps until closure of the valves. The existing and new safety valve mechanism closes, i.e. reaches the end position, after approximately 3 and 1.8 ms, respectively. Since the FSI simulations of the new passive air blast safety valve were carried out during the design of experiment process before manufacturing the prototype and the final geometrical optimizations, the shape of the valve and closing mechanism in the simulations is slightly different from the final design. However, this is not regarded critical for the outcome of the results, since the closing time and the flow cross section remained similar.

First of all, when considering the pressure distribution (see Fig. B.13), the incident shock wave traveling from left to right with a magnitude of approximately 1 bar is visible at t = −0.2 ms. Due to the small flow cross section in the existing design, an almost normal reflection of the blast wave occurs (see Fig. B.13a, t = 0.2 ms), which results in reflected pressures of up to 3.15 bar (t = 0.6 ms). More complex reflections are present in the novel valve design while reaching pressures of up to 4 bar. Due to the increased flow cross section of the novel valve design, the main blast pressure leakage (see Fig. B.13b, visible from t = 0.6 to 1.8 ms, right hand side of the valve) has a magnitude of approximately 0.8 bar, which is roughly twice as high compared to the existing design. Moreover, subsequent smaller pressure waves with magnitudes of 0.1 to 0.2 bar are passing both safety valves (visible from t = 1.4 to 2.6 ms, on the right hand side close to the valves). Both phenomena are in accordance with the registered pressure–time distribution at measuring location 2 (compare Fig. 10), revealing a first large pressure peak and subsequent reduced pressure fluctuations.

When evaluating the velocity field of the existing valve design (see Fig. B.14a), the fluid reaches a velocity of approximately 580 m/s at t = 0.2 ms and is subsequently reduced until valve closure (t = 3 ms). Inversely, due to the increased flow cross section, the air velocity in the new valve design is first lower (approximately 175 m/s, see Fig. B.14b, t = 0.2 ms) and reaches 600 m/s when approaching the closed state (t = 1.8 ms). As mentioned in Section 4.3, the new closing mechanism is not modeled fully closed in the simulation due to mesh deformation issues, which explains the remaining increased air flow after closure from 2.2 to 3 ms. Interestingly, in comparison to the ventilation operation (see Section 7.2) and probably due to the significant bending of the metal sheets, the air flow is more complex in the novel valve design with increased flow deflection and separation, e.g. at t = 1.4 ms. This behavior most likely enhances the residual pressure fluctuations discussed beforehand.

References

Joint Committee for Guides in Metrology (JCGM), 2008. Evaluation of measurement data – guide to the expression of uncertainty in measurement, ISO/IEC guide 98-3.

ANSYS®, 2017. ANSYS CFX release 18.2 documentation.

Dassault Systèmes, 2018. ABAQUS release 2018 documentation.

Benra, F.K., Dohmen, H.J., Pei, J., Schuster, S., Wan, B., 2011. A comparison of one-way and two-way coupling methods for numerical analysis of fluid-structure interactions. J. Appl. Math. 2011, http://dx.doi.org/10.1155/2011/853560.

Børvik, T., Hanssen, A.G., Langseth, M., Olovsson, L., 2009. Response of structures to planar blast loads - A finite element engineering approach. Comput. Struct. 87 (9–10), 507–520. http://dx.doi.org/10.1016/j.compstruc.2009.02.005.

Faucher, V., Casadei, F., Valsamos, G., Larcher, M., 2019. High resolution adaptive framework for fast transient fluid-structure interaction with interfaces and structural failure ? Application to failing tanks under impact. Int. J. Impact Eng. 127, 62–85. http://dx.doi.org/10.1016/j.ijimpeng.2018.10.008.

Ha, S.T., Ngo, L.C., Saeed, M., Jeon, B.J., Choi, H., 2017. A comparative study between partitioned and monolithic methods for the problems with 3D fluid-structure interaction of blood vessels. J. Mech. Sci. Technol. 31 (1), 281–287. http://dx.doi.org/10.1007/s12206-016-1230-2.

Henchie, T.F., Chung Kim Yuen, S., Nurick, G.N., Ranwaha, N., Balden, V.H., 2014. The response of circular plates to repeated uniform blast loads: An experimental and numerical study. Int. J. Impact Eng. 74, 36–45. http://dx.doi.org/10.1016/j.ijimpeng.2014.02.021.

Kambouchev, N., Noels, L., Radovitzky, R., 2007. Numerical simulation of the fluid-structure interaction between air blast waves and free-standing plates. Comput. Struct. 85 (11–14), 923–931. http://dx.doi.org/10.1016/j.compstruc.2006.11.005.

Khawaja, H.A., Messahel, R., Ewan, B., Mhamed, S., Moatamedi, M., 2016. Experimental and numerical study of pressure in a shock tube. J. Pressure Vessel Technol. Trans. ASME 138 (4), 041301. http://dx.doi.org/10.1115/1.4031591.

Kim, D.W., Kim, T.H., Kim, H.D., 2017. A study on characteristics of shock train inside a shock tube. Theor. Appl. Mech. Lett. 7 (6), 366–371. http://dx.doi.org/10.1016/j.taml.2017.09.005.

Kumar, R., Nedungadi, A., 2020. Using gas-driven shock tubes to produce blast wave signatures. Front. Neurol. 11, 90. http://dx.doi.org/10.3389/fneur.2020.00090.

Louar, M.A., Belkassem, B., Ousji, H., Spranghers, K., Kakogiannis, D., Pyl, L., Vantomme, J., 2015. Explosive driven shock tube loading of aluminium plates: Experimental study. Int. J. Impact Eng. 86, 111–123. http://dx.doi.org/10.1016/j.ijimpeng.2015.07.013.

Malhotra, A., Carson, D., McFadden, S., 2017. Blast pressure leakage into buildings and effects on humans. In: Procedia Engineering, Vol. 210. Elsevier Ltd, pp. 386–392. http://dx.doi.org/10.1016/j.proeng.2017.11.092.

Menter, F.R., 1994. Two-equation eddy-viscosity turbulence models for engineering applications. AIAA J. 32 (8), 1598–1605. http://dx.doi.org/10.2514/3.12149.

Mo, C., Zeng, X., Xiang, K., 2015. The passive blast protection valve flow field numerical simulation and movement analysis. In: 4th International Conference on Mechatronics, Materials, Chemistry and Computer Engineering. Atlantis Press, pp. 482–489. http://dx.doi.org/10.2991/icmmcce-15.2015.97.

Nguyen, V.T., Gatzhammer, B., 2015. A fluid structure interactions partitioned approach for simulations of explosive impacts on deformable structures. Int. J. Impact Eng. 80, 65–75. http://dx.doi.org/10.1016/j.ijimpeng.2015.01.008.

Rigas, F., Sklavounos, S., 2005. Experimentally validated 3-D simulation of shock waves generated by dense explosives in confined complex geometries. J. Hard Mater. 121 (1–3), 23–30. http://dx.doi.org/10.1016/j.jhazmat.2005.01.031.

Sharma, P.K., Patel, B.P., Lal, H., 2016. Blast valve design and related studies: A review. Defence Sci. J. 66 (3), 242–250. http://dx.doi.org/10.14429/dsj.66.9618.

Sharma, P.K., Patel, B.P., Lal, H., 2017. On the response of hemispherical shell under blast loading. In: Procedia Engineering, Vol. 173. Elsevier Ltd, pp. 533–538. http://dx.doi.org/10.1016/j.proeng.2016.12.085.

Singh, G.P., Sharma, J.D., Arora, R., Sandhu, I.S., 2020. CFD analysis of shock tube for blast impact testing. In: Materials Today: Proceedings, Vol. 28. Elsevier Ltd, pp. 1872–1878. http://dx.doi.org/10.1016/j.matpr.2020.05.294.

Spranghers, K., Vasilakos, I., Lecompte, D., Sol, H., Vantomme, J., 2013. Numerical simulation and experimental validation of the dynamic response of aluminum plates under free air explosions. Int. J. Impact Eng. 54, 83–95. http://dx.doi.org/10.1016/j.ijimpeng.2012.10.014.

Subramaniam, K.V., Nian, W., Andreopoulos, Y., 2009. Blast response simulation of an elastic structure: Evaluation of the fluid-structure interaction effect. Int. J. Impact Eng. 36 (7), 965–974. http://dx.doi.org/10.1016/j.ijimpeng.2009.01.001.

Yang, Y., Liou, W.W., Sheng, J., Gorsich, D., Arepally, S., 2013. Shock wave impact simulation of a vehicle occupant using fluid/structure/dynamics interactions. Int. J. Impact Eng. 52, 11–22. http://dx.doi.org/10.1016/j.ijimpeng.2012.09.002.

Yuan, Y., Tan, P.J., Shojaei, K.A., Wrobel, P., 2017. The influence of deformation limits on fluid-structure interactions in underwater blasts. Int. J. Impact Eng. 101, 9–23. http://dx.doi.org/10.1016/j.ijimpeng.2016.11.007.

Zalosh, R.G., 2014. Appendix c: Blast waves. In: Industrial Fire Protection Engineering. John Wiley & Sons, Ltd, Chichester, UK, pp. 375–380. http://dx.doi.org/10.1002/9781118903117.app3.